Creep–Fatigue Interaction of P91 Steam Piping Subjected to Typical Start-up and Shutdown Cycles

Smith Salifu[1,*], Dawood Desai[1] & Schalk Kok[2]

[1]Department of Mechanical and Automation Engineering, Tshwane University of Technology, Pretoria, South Africa

[2]Department of Mechanical and Aeronautical Engineering, University of Pretoria, Pretoria, South Africa

Correspondence to Smith Salifu. e-mail: smithsalifu@gmail.com

Abstract

The possibility of creep–fatigue interaction occurring in steam pipes of power generation plants during operation has been on the front burner for years. Often, failure of the pipes during operation is attributed to either creep alone or fatigue alone. Of recent, some failures are speculated to be due to simultaneously coupled interaction between creep and fatigue, especially when the failure occurs earlier than anticipated. The literature shows that such studies are very limited and indeed under-researched. Thus, there is a dire need to systematically investigate this coupled creep–fatigue phenomenon and provide clarity as the failure of high-pressure steam piping has consequential and very significant effects on the suppliers and end users. In this work, a special Fortran user subroutine script of a phenomenological modified hyperbolic sine creep model was developed and implemented in Abaqus CAE/2019 finite element code to initially determine the creep behavior of a P91 steam piping network subjected to a typical daily start-up and shutdown cycle. Subsequently, fe-safe/TURBOlife software was employed to investigate whether the failure induced by the start-up and shutdown cycles was due to fatigue alone, creep alone or due to creep–fatigue interaction. Interestingly, the study showed that the failure of the piping network under the specified operating conditions is specifically due to creep alone. Furthermore, the intrados of the elbow in the piping network was identified as the region most prone to failure, and the piping network will only survive a total of 7.1 and 7.7 years under these operating conditions for both machined and fine-machined surfaces, respectively. These results were thereafter analytically validated, and it showed a strong correlation with the numerically determined creep rate.

Keywords: Abaqus CAE/2019; Finite element analysis; Creep rate; Creep–fatigue interaction; fe-safe/TURBOlife; Intrados

Introduction

In an attempt to improve the efficiency in energy production and also to comply with the ever-increasing demand for cleaner and sustainable electrical energy, the operating pressure and temperature of power plant components are increased. In addition to the increase in the operating parameters of these components, they are sometimes subjected to abnormal operation cycle emanating from the quest to strike a balance between supply

and distribution during peak and off-peak periods [1]. The unusual cycle consists of several start-up phases closely followed by a steady or constant high temperature and pressure application and then the shutdown phases [2]. Thus, the components are invariably subjected to operation in creep–fatigue regime and failure due to creep–fatigue damage is presumed to be imminent [3]. Creep is an already well-established failure mode for components subjected to operation at elevated temperatures. However, the failure mode becomes more complicated when the component is subjected to high operating temperature and variation in the loading conditions [1].

Creep–fatigue interaction describes the situation where the accumulated rate of damage under complex loading differs from the linear summation of the rate of damages produced by cyclic and creep components [3, 4]. Microstructurally, creep–fatigue interaction is depicted as a combination of effects from creep damage and fatigue damage. While fatigue failure is manifested due to crack damage, creep is manifested by cavitation damage via the formation of creep voids on the interior grain boundaries. Therefore, in the presence of damage due to creep–fatigue interaction, creep cavitation in addition to surface fatigue damage may be found within the material under consideration and the interaction or coupling of these damage modes encourages an accelerated failure such that the failure path will exhibit a mixed trans and intergranular path.

Limited research work has been carried out in a creep–fatigue environment with a view to investigating the possibility of creep–fatigue interactions occurring [1, 5–7], yet, there are still profuse controversies as regards the failure mode particularly in the power generation sector where the start-up and shutdown cycles are presumed be insufficient to induce fatigue failure [8]. The behavior of materials subjected to creep–fatigue interaction environment is often simulated in the laboratory via high temperature, low cycle fatigue tests that considers the hold time at constant stress or strain. Different factors such as strain rate, strain range, hold time and temperature on the creep–fatigue resistance of materials are often determined by the tests in order to develop realistic design codes for materials under specified conditions [3].

Due to the advancement in computer technology, numerical simulation provides an effective method to assess the creep and fatigue behavior, and profuse research [6, 9–11] has been carried out to determine the creep behavior under different models using finite element (FE) simulation. Also, investigation involving fatigue behaviour utilizing FE simulations has also been conducted by many researchers [1, 12–14], but the development of creep–fatigue models capable of being implemented in FE simulations is limited in the open literature. Most of the creep–fatigue damages considered were by simple addition of the individual creep and fatigue damage together. This linear summation method fails to account for the creep–fatigue interaction, thus rendering the results obtained somewhat unreasonable in an environment with possibility of creep–fatigue interaction. Hence, the ability to account for possible coupled creep–fatigue interaction is crucial to gaining a more conservative life prediction.

In order to incorporate the effect of creep–fatigue interaction, time fraction rules were recommended by the current prevailing standards such as RCC-MR [15] and ASME BPVC [16], while the ductility exhaustion approach is used by R5 standard [17]. The ability to

understand the damage evolution, particularly the interaction damage in a creep–fatigue environment, plays a crucial role in the determination of the structural integrity of components at elevated temperatures [18, 19].

In this paper, the creep–fatigue interaction of P91 (9Cr–1Mo–V) power generation steam piping network subjected to real-life start-up and shutdown cycles initiated by peak and off-peak periods demand during supply was determined. The FE simulation to determine the thermomechanical/creep behavior was conducted using FE analysis code, Abaqus CAE/2019, while the possibility of creep–fatigue interaction occurring during operation was subsequently determined using the R5 standard ductility exhaustion approach employed in fe-safe/TURBOlife software.

Thermo-mechanical Stress Model Developed in a Straight Pipe

When a pipe or thick-wall cylinder is subjected to internal pressure, three principal stresses, namely hoop or circumferential stress σ_t, radial stress σ_r and longitudinal or axial stress σ_z, are generated. Longitudinal stress developed is due to the pressure thrust on the heads of the pipe or cylinder. The value of the radial and hoop stress varies throughout the entire cylinder, whereas the value of the longitudinal stress is constant all through [20]. The expression for circumferential, radial and axial stresses of a thick-wall cylinder with external radius and internal radius r_0 and r_1, and subjected to internal pressure, P, was introduced by Lame´ [21] as shown in Eqs 1, 2 and 3.

$$\sigma_{\mathrm{r}} = P\frac{r_{\mathrm{i}}^2\left(r^2 - r_o^2\right)}{r^2\left(r_o^2 - r_{\mathrm{i}}^2\right)} \quad \text{(Eq 1)}$$

$$\sigma_t = P\frac{r_{\mathrm{i}}^2\left(r^2 + r_o^2\right)}{r^2\left(r_o^2 - r_{\mathrm{i}}^2\right)} \quad \text{(Eq 2)}$$

$$\sigma_z = \frac{P_{\mathrm{i}} r_{\mathrm{i}}^2}{r_o^2 - r_{\mathrm{i}}^2} \quad \text{(Eq 3)}$$

The effective mechanical stress, σ_m, developed in the pipe during operation can be obtained using von Mises theory as shown in Eq 4.

$$\sigma_{\mathrm{m}} = \sqrt{\left[\sigma_t^2 + \sigma_{\mathrm{r}}^2 + \sigma_z^2 - \left(\sigma_t\sigma_{\mathrm{r}} + \sigma_t\sigma_z + \sigma_{\mathrm{r}}\sigma_z\right)\right]} \quad \text{(Eq 4)}$$

Also, for a straight thick pipe with external radius and internal radius r_o and r_i subjected to operation at elevated temperature [22, 23], the thermal stress developed is given by the following expressions:

$$\sigma_{\mathrm{tT}} = \frac{\alpha E}{(1-\nu)r^2}\left[\frac{r^2 + r_{\mathrm{i}}^2}{r_o^2 - r_{\mathrm{i}}^2}\int_{r_{\mathrm{i}}}^{r_o} Tr\mathrm{d}r - \int_{r_{\mathrm{i}}}^{r} Tr\mathrm{d}r - Tr^2\right] \quad \text{(Eq 5)}$$

$$\sigma_{\mathrm{rT}} = \frac{\alpha E}{(1-\nu)r^2}\left[\frac{r^2 - r_{\mathrm{i}}^2}{r_o^2 - r_{\mathrm{i}}^2}\int_{r_{\mathrm{i}}}^{r_o} Tr\mathrm{d}r - \int_{r_{\mathrm{i}}}^{r} Tr\mathrm{d}r\right] \quad \text{(Eq 6)}$$

$$\sigma_{\mathrm{zT}} = \frac{\alpha E}{(1-\nu)}\left[\frac{2}{r_o^2 - r_{\mathrm{i}}^2}\int_{r_{\mathrm{i}}}^{r_o} Tr\mathrm{d}r - T\right] \quad \text{(Eq 7)}$$

Using von Mises theory, the effective thermal stress is determined.

$$\sigma_{\mathrm{T}} = \sqrt{\left[\sigma_t^2 + \sigma_{\mathrm{r}}^2 + \sigma_z^2 - (\sigma_t\sigma_{\mathrm{r}} + \sigma_t\sigma_z + \sigma_{\mathrm{r}}\sigma_z)\right]} \quad \text{(Eq 8)}$$

where σ_r is the radial mechanical stress, σ_t is the circumferential mechanical stress, σ_z is axial mechanical stress, σ_{rT} is the thermal radial stress, σ_{tT} thermal circumferential stress, σ_{zT} is thermal axial stress, σ_m is the effective mechanical von Mises stress, and σ_T is effective thermal von Mises stress.

Thus, the thermo-mechanical stress, σ_{TM}, induced in a straight pipe subjected to operation in both thermal and mechanical environment is determined by the by the summation of the effective mechanical and thermal stresses.

$$\sigma_{\mathrm{TM}} = \sigma_{\mathrm{m}} + \sigma_{\mathrm{T}} \quad \text{(Eq 9)}$$

Creep–Fatigue Damage Model

Modified Hyperbolic Sine Creep Model

The next generation of creep strain rate expression that can describe creep rate over a whole range of stress was proposed by Garofalo [24, 25] under creep conditions and Sellars and Tegart [25], under hot deformation conditions. The expression known as the modified hyperbolic sine creep law encompasses both high- and low-stress regime, and it is given by

$$\dot{\varepsilon}_{\mathrm{cr}} = A[\sinh(\sigma H)]^n \exp\left[\frac{-Q}{RT}\right] \quad \text{(Eq 10)}$$

where *A, n* and *H* are material constants, *Q* is activation energy, T is temperature, and R is gas constant.

Creep Damage Model

Based on the ductility exhaustion theory, it is assumed that the local strain in a component subjected to operation in a creep regime reaches critical ductility such that there is forward propagation of a crack [19, 26]. As such, the rate of creep strain damage or creep strain rate damage can be determined by the ratio of the current creep strain rate to the creep strain at failure as shown in Eq 11.

$$d_{\mathrm{c}} = \frac{\varepsilon_{\mathrm{c}}}{\varepsilon_{\mathrm{f}}^*} \quad \text{(Eq 11)}$$

where d_c, ε_c and ε_f^* are the creep damage rate, creep strain rate and the multiaxial creep failure strain, respectively.

The complex nature of strain state at the elbows of the piping network, ε_f^*, is different from the uniaxial creep strain, ε_f . Hence, it is essential to establish an appropriate relationship between them in order to calculate the creep damage. Several multiaxial creep ductility factors (MCDFs) that show the ratio of failure of multiaxial creep strain against uniaxial creep strain have been proposed. With respect to the coalescence theory and cavity growth, the MCDF was proposed by Wen [27], and it is defined as:

$$\frac{\varepsilon_f^*}{\varepsilon_f} = \exp\left[\frac{2}{3}\left(\frac{n-0.5}{n+0.5}\right)\right] \Big/ \exp\left[2\left(\frac{n-0.5}{n+0.5}\right)\frac{\sigma_m}{\sigma_e}\right] \quad \text{(Eq 12)}$$

where n is material constant and rm is hydrostatic stress.

When compared to other MCDFs, the accuracy of the multiaxial creep strain obtained by this model is higher [27].

Fatigue Damage Model

Based on the principle of thermodynamic [3, 28], low cycle fatigue can be calculated as defined below:

$$\frac{d_f}{dN} = \frac{R_v}{\varphi(\gamma+1)}\frac{(\Delta p)^{\gamma+1}}{(1-\omega)^{\alpha_0}} \quad \text{(Eq 13)}$$

where φ, γ and α_0 are material constants, R_v represents stress triaxiality effect, d_f is fatigue damage, and Δ_p is the plastic strain accumulated in one cycle and can be obtained using the Ramberg–Osgood equation [1, 29]:

$$\frac{\Delta\sigma_e}{2} = K'\left(\frac{\Delta p}{2}\right)^{n'} \quad \text{(Eq 14)}$$

where n' and K' are material constants and $\Delta\sigma_e$ represents equivalent stress variation in one complete cycle.

Sequel to the difference in the damage mechanism for creep and fatigue, the stress triaxiality on both damage phenomena differs; thus, R_v is given by

$$R_v = \frac{2}{3}(1-v) + 3(1-2v)\left(\frac{\sigma_m}{\sigma_e}\right)^2 \quad \text{(Eq 15)}$$

where v represents the Poisson ratio.

Creep–Fatigue Interaction

In order to determine the damage caused due to creep–fatigue interaction, a creep–fatigue interaction term was proposed by Lagneborg [30], and it is defined as:

$$d_{cf} = b((d_f/dN)(d_c/dN))^{1/2} \quad \text{(Eq 16)}$$

where d_{cf} is damage due to creep–fatigue interaction and b is creep–fatigue interaction coefficient, which is a function of loading conditions, temperature, hold time, etc. The d_f/dN term represents the fatigue damage obtained in one cycle as expressed in Eqs 13, 14 and 15, while the term d_c/dN represents the creep damage accumulated during one complete cycle. The accumulated creep damage in
Eq 11 can be expressed as

$$\frac{d_c}{dN} = \int_0^{t_h} d_c \, dt \quad \text{(Eq 17)}$$

where t_h represents the hold time in one complete cycle. Thus, the creep–fatigue interaction damage model [3] can be given by

$$\frac{d_{cf}}{dN} = \frac{d_c}{dN} + \frac{d_f}{dN} + b\left(\left(\frac{d_c}{dN}\right)\left(\frac{d_f}{dN}\right)\right)^{1/2} \quad \text{(Eq 18)}$$

Model Verification

Based on the constitutive models discussed in the previous section, a FE model for the heat transfer, thermo-mechanical and creep was developed using Abaqus CAE/2019 software, while the creep–fatigue interaction was computed using fe-safe/TURBOlife software based on the output database results from the preceding Abaqus model. The modified hyperbolic sine creep model script was developed in Fortran and implemented in the Abaqus model via a user subroutine, while the accumulated damage, creep life and creep–fatigue life were computed in fe-safe/TURBOlife software.

FE Model

In order to capture a detailed behavior of creep and creep–fatigue interaction of a power generation plant steam piping network in service, a three-dimensional (3D) model of the real piping network and its insulation jacket was developed in Abaqus CAE/2019 as shown in Figs. 1 and 2, while the assembly model is shown in Fig. 3.

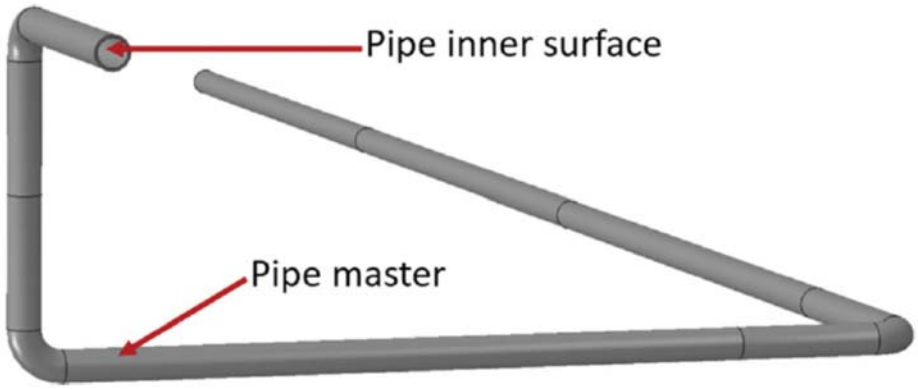

Fig. 1 Piping network model

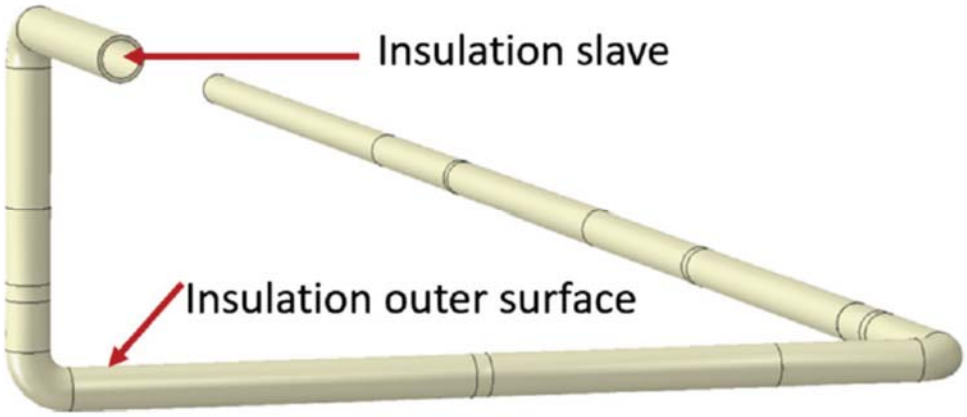

Fig. 2 Insulation jacket model

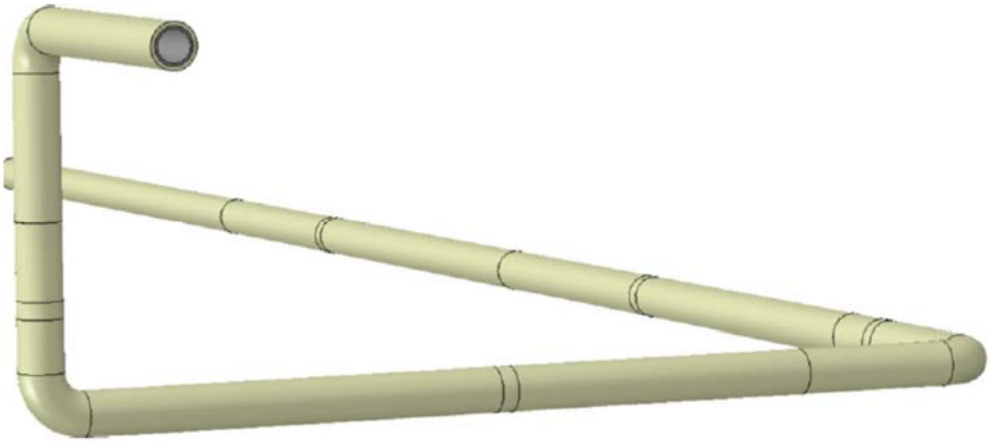

Fig. 3 Pipe-insulation jacket assembly

The dimensions of the steam piping network and pyrogel insulation jacket used in this analysis are shown in Tables 1 and 2. The analysis was carried out in a sequentially coupled manner by first conducting a heat transfer analysis before the thermo-mechanical/creep analysis because the applied temperature influences the stress developed in the subsequent analysis but not vice versa [31].

Table 1 Dimensions of steel pipe [32]

Total length of pipe (m)	Internal diameter (m)	External diameter (m)	Radius of elbow (m)	Thickness of pipe (m)
52.1	0.38	0.44	0.50	0.03

Table 2 Dimensions of pyrogel insulation jacket [33, 34]

Total length of insulation (m)	Internal diameter of insulation (m)	External diameter of insulation (m)	Radius of elbow (m)	Thickness of insulation (m)
52.10	0.44	0.54	0.50	0.05

A suitable FE mesh size used was determined after conducting a mesh convergence study that is based on the thermo-mechanical stress developed by the assembly under operational conditions. Upon completion of the study, a global seed size of 50 mm with a total of 92 196 DC3D8 element type for heat transfer and 92 196 C3D8R element type for the creep/creep–fatigue analysis was observed to be suitable. For the heat transfer analysis, a sink temperature load (operating temperature) of 550°C with a film coefficient of 10,000 W/m^2K was applied to inner surface of the pipe-insulation assembly, while a sink temperature (room temperature) of 25°C with air convective heat transfer coefficient of 18 W/m^2K was applied to the outer surface of the pipe-insulation assembly [34]. During the thermo-mechanical/creep simulation, a typical operating pressure of 18 MPa was applied to the inner surface of the assembly and appropriate mechanical (displacement/rotation) boundary conditions were applied to the pipeinsulation assembly such that the assembly is able to be displaced in the U1, U2 and U3 and rotate in UR1, UR2 and UR3 at the elbows as shown in Fig. 4.

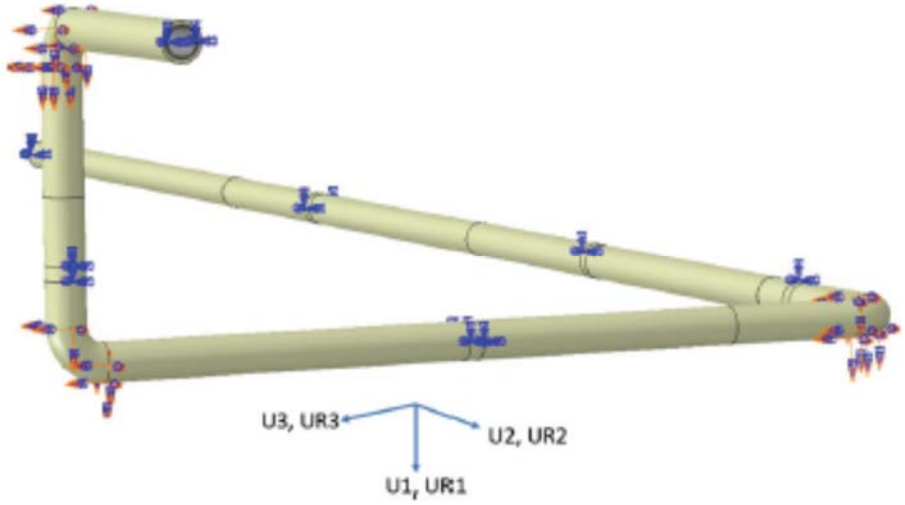

Fig. 4 Applied boundary conditions on pipe-insulation jacket assembly

Parameters for Creep/Creep–Fatigue Damage Model

The temperature-dependent elastic–plastic and thermal properties of P91 steel shown in Figs. 5, 6 and 7, with Poisson's ratio of 0.33 and conductivity of 33 W/mK are implemented into the FE model. The uniaxial data of P91 steel creep test conducted at 550°C [35] were used to generate the parameters for the phenomenologically modified hyperbolic sine creep model used in this analysis. The values of the constants were obtained through curve fitting and were implemented via the Fortran creep user subroutine script developed for the modified hyperbolic sine creep model. Table 3 shows the modified hyperbolic sine creep parameters/constants used for this analysis. Also, the TURBOlife properties, Neuber plasticity method with elastic follow-up factor of 0.33, ductility exhaustion and Morrow correction algorithm [8] were implemented in fesafe/TURBOlife software to determine the creep damage and possible creep–fatigue interaction. In the analysis, two different surface finishes, namely machined finish ($16 < Ra \leq 40$ µm) and finely machined finish surface ($4 < Ra \leq 16$), were considered. Also, real case scenario of 24-h operational loading cycle consisting of a total of 6-h peak period with steady-state operation, 14-h off-peak period with steady-state down time and 4-h transient state as shown in Fig. 8 was used in this analysis.

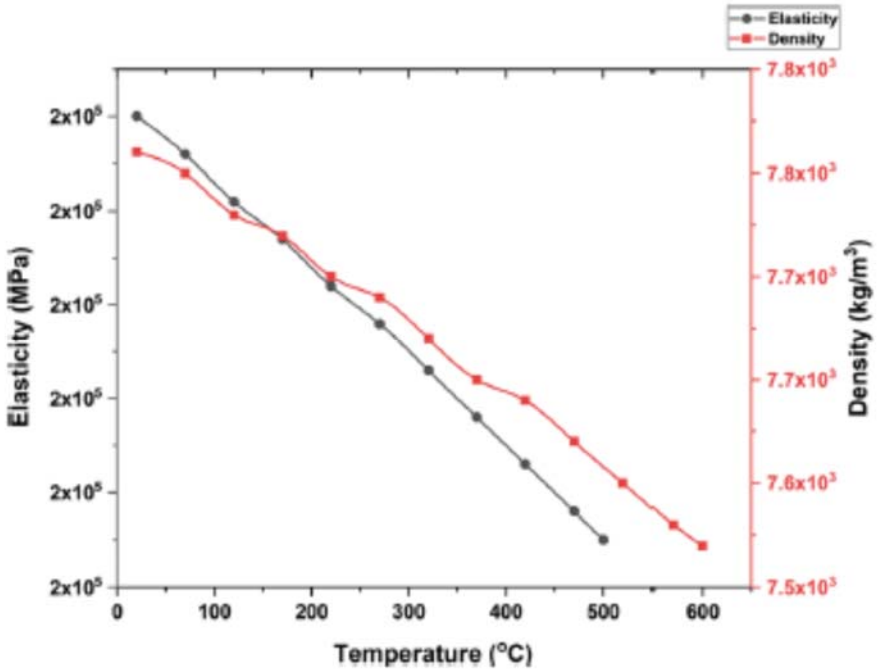

Fig. 5 Elasticity and density of P91 steel as a function of temperature

Table 3 Modified hyperbolic sine creep constant for P91 steel at 550 °C [35]

A ($\times 10^{29}$/h)	H ($\times 10^{-8}$ Pa)	n	Q (J/(mol·K))	R (J/mol)	T (K)
3.50	2.37	1.32	599,342.4	8.314	823

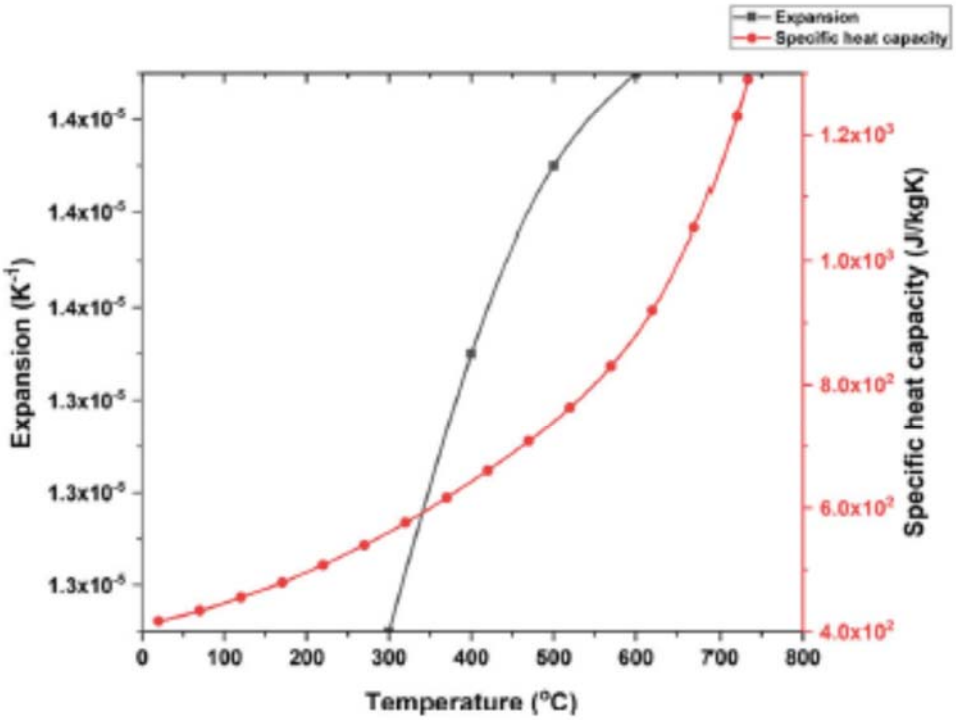

Fig. 6 Expansion and specific heat capacity of P91 steel as a function of temperature

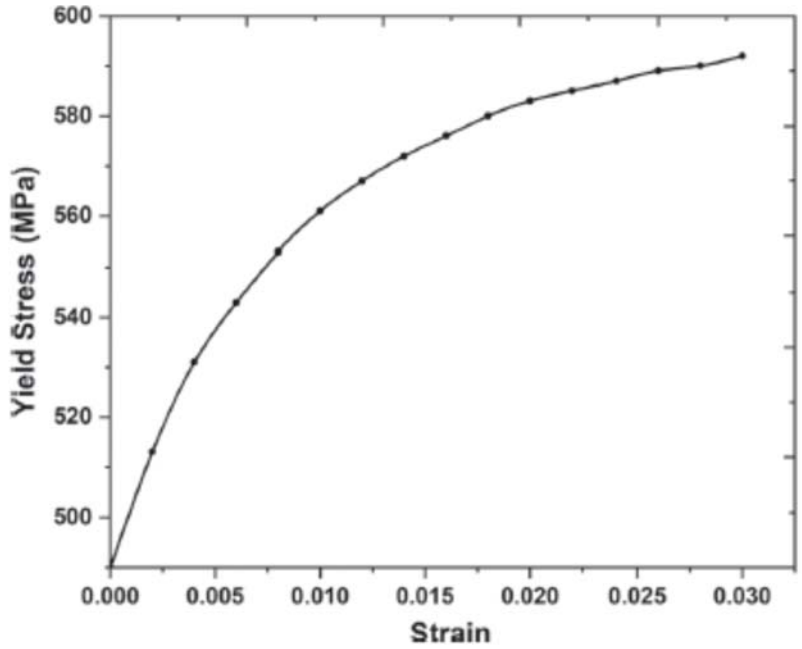

Fig. 7 Plasticity of P91 steel

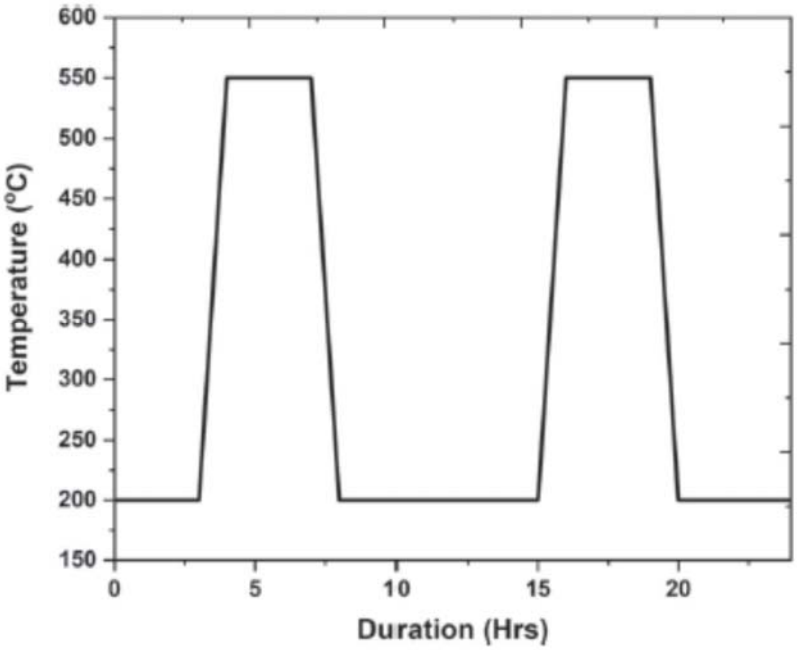

Fig. 8 Operational cycle

Results and Discussions

From the mesh convergence study conducted, a 50-mm mesh size with a total of 92,126 elements and 155,162 nodes was found suitable for the analysis. Figure 9 shows the graph obtained from the study, while the assembled FE model mesh is shown in Fig. 10.

The contour plot of the temperature distribution profile obtained from the heat transfer analysis is displayed in Fig. 11. The maximum operating temperature was maintained in the interior of pipe-insulation assembly, and the least temperature of the assembly with a value

of 42.9°C was developed on the outer surface of the insulation jacket as expected. This is an indication that pyrogel is a suitable insulation jacket for steam pipes and the thickness of the jacket determine the extent to which it can reduce the outer surface temperature of the assembly [34].

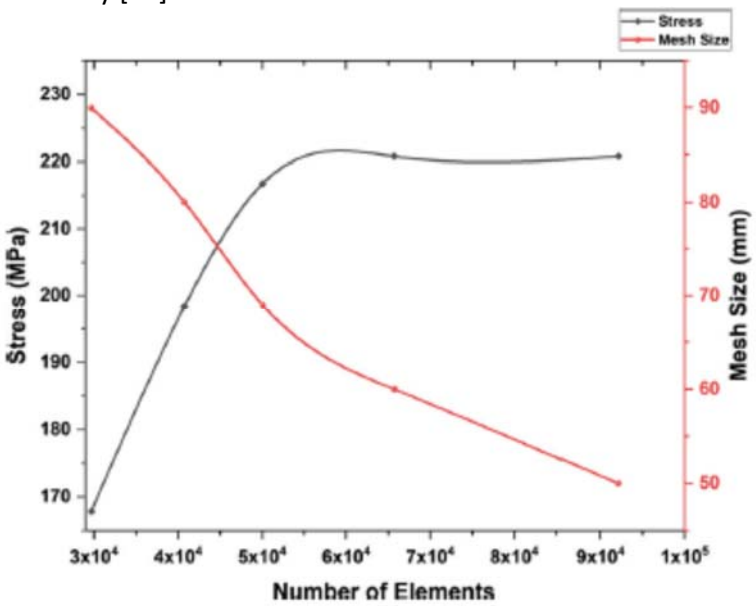

Fig. 9 Mesh convergence study graph

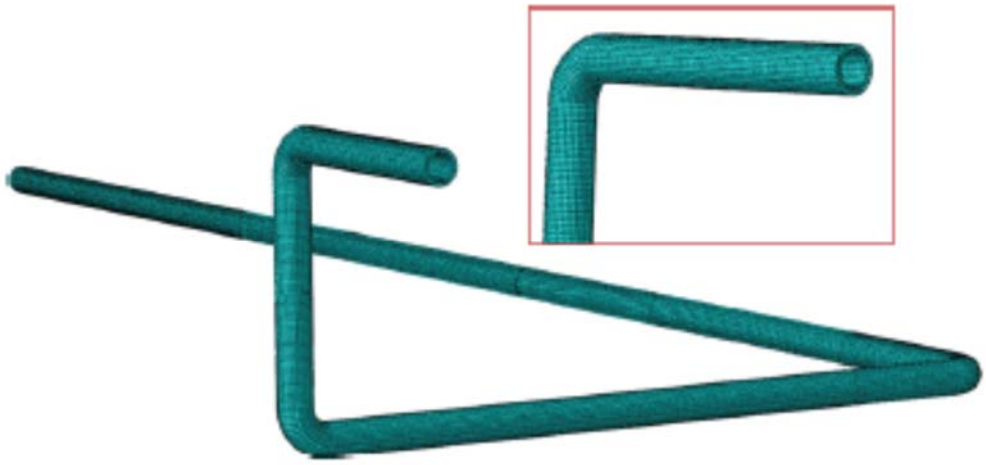

Fig. 10 Pipe-insulation jacket assembly mesh

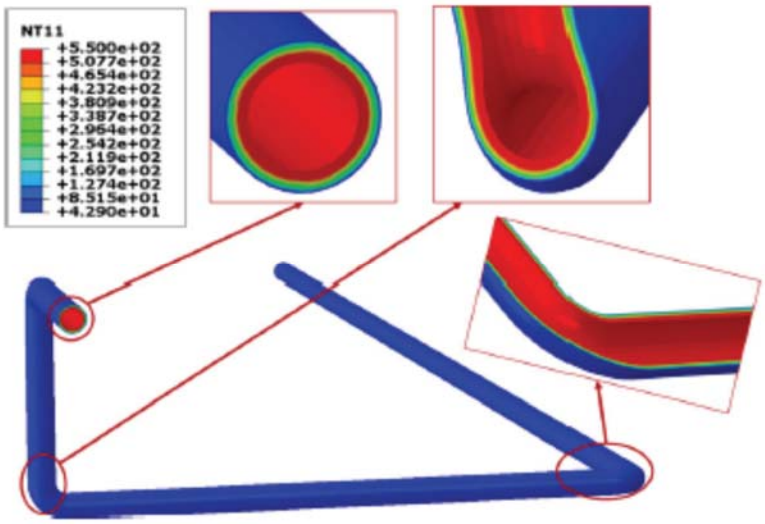

Fig. 11 Contour plot for temperature distribution profile

The contour plot for the developed creep stress and strain rate in the pipe when it is subjected to the specified operational condition is depicted in Figs. 12 and 13, respectively, while the results of the simulated creep stress and strain at the straight region of the piping network are shown in Fig. 14. Under the specified condition, a maximum stress of 220.2 MPa with strain rate of 1:076 X 10^{-5} /h was developed at the intrados of the piping network's elbows. This indicates that the failure of the network will originate from the intrados of the network as expected. It was also observed that plastic strain was not developed during operation irrespective of the start-up and shutdown cycle the pipe was subjected to.

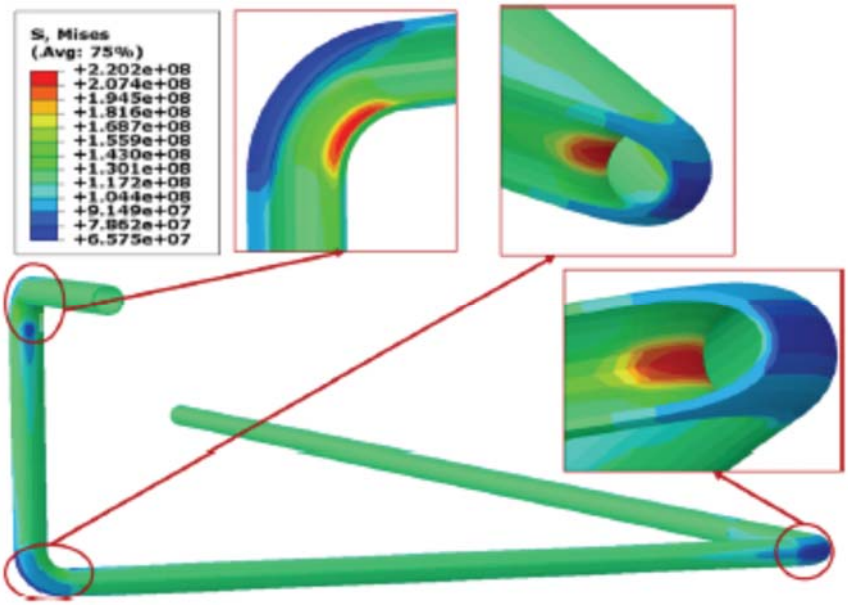

Fig. 12 Contour plot for creep stress

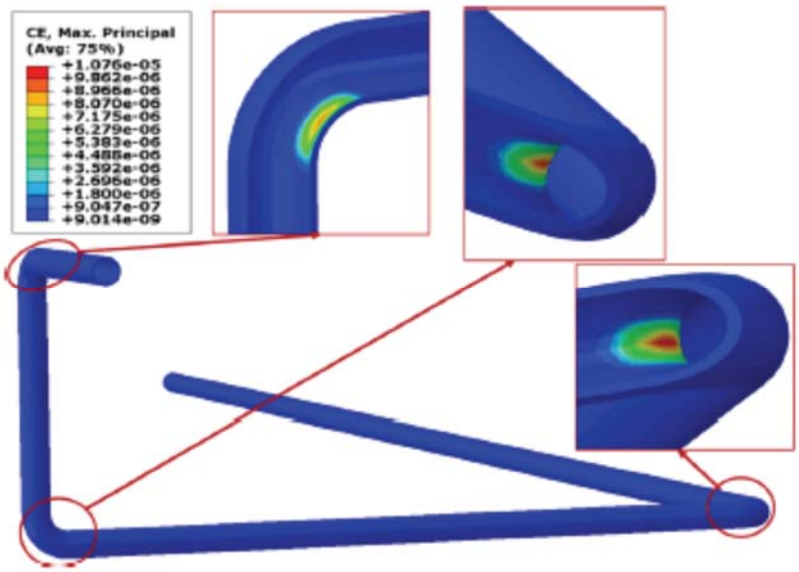

Fig. 13 Contour plot for creep strain rate

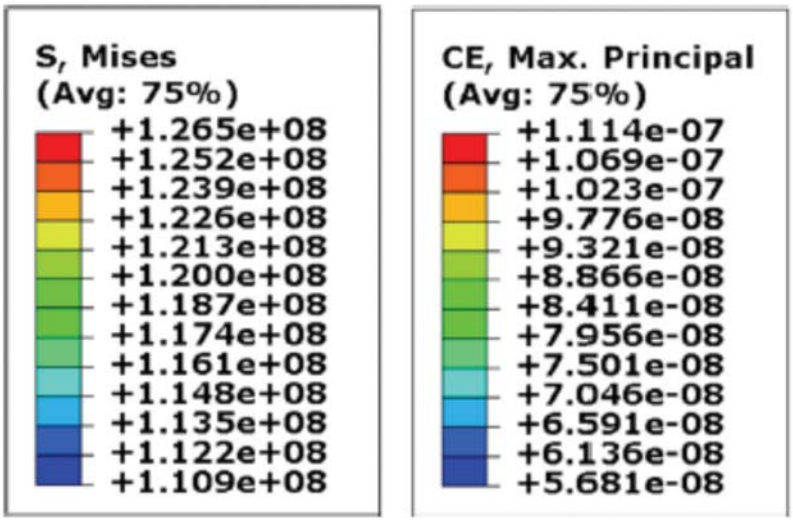

Fig. 14 Result of creep stress and strain rate at the straight region of the piping network

Figure 15 depicts the contour plot and result obtained from the creep–fatigue analysis carried out using fe-safe/TURBOlife software for machined finish surface, while the plot for the fine-machined finish surface is shown in Fig. 16. The results indicate that the failure of the piping network with both surface finishing is strictly due to creep alone. This can be attributed to the inability of plastic strain to be developed during operation regardless of the start-up and shutdown cycles the piping network was subjected to. However, extensive plastic strain is required for failure due to fatigue to occur in a component [36], and the operating cycles the piping network was subjected to were insufficient to induce such strain.

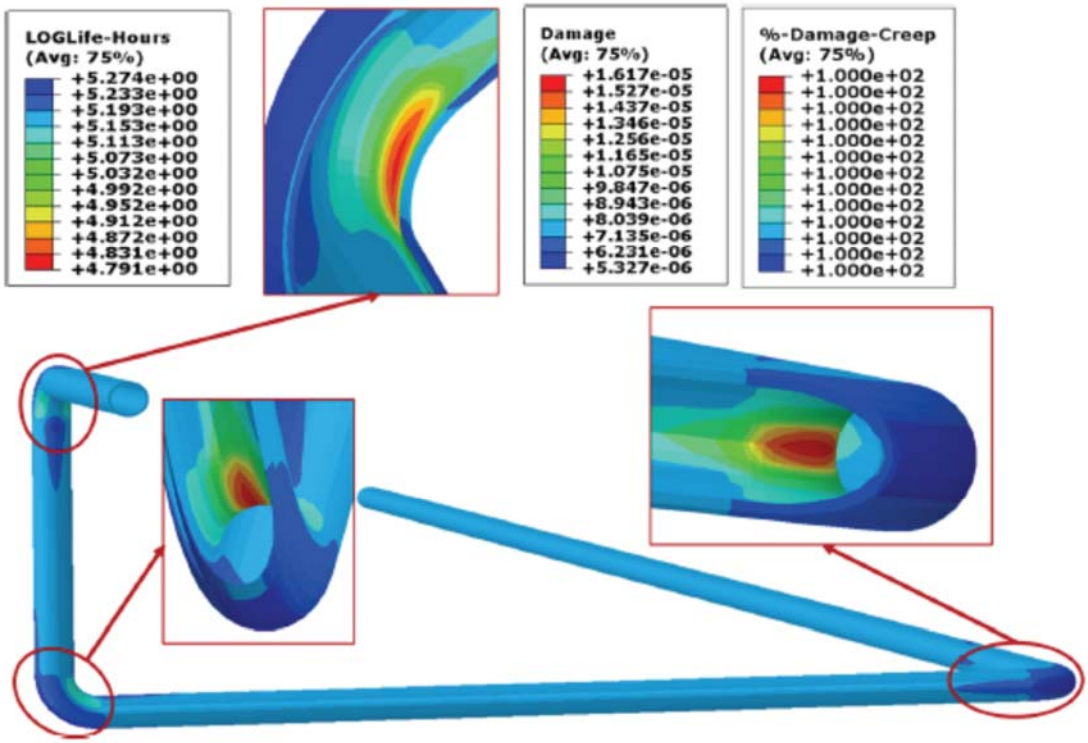

Fig. 15 Contour plot for creep life and damage for machined finished surface

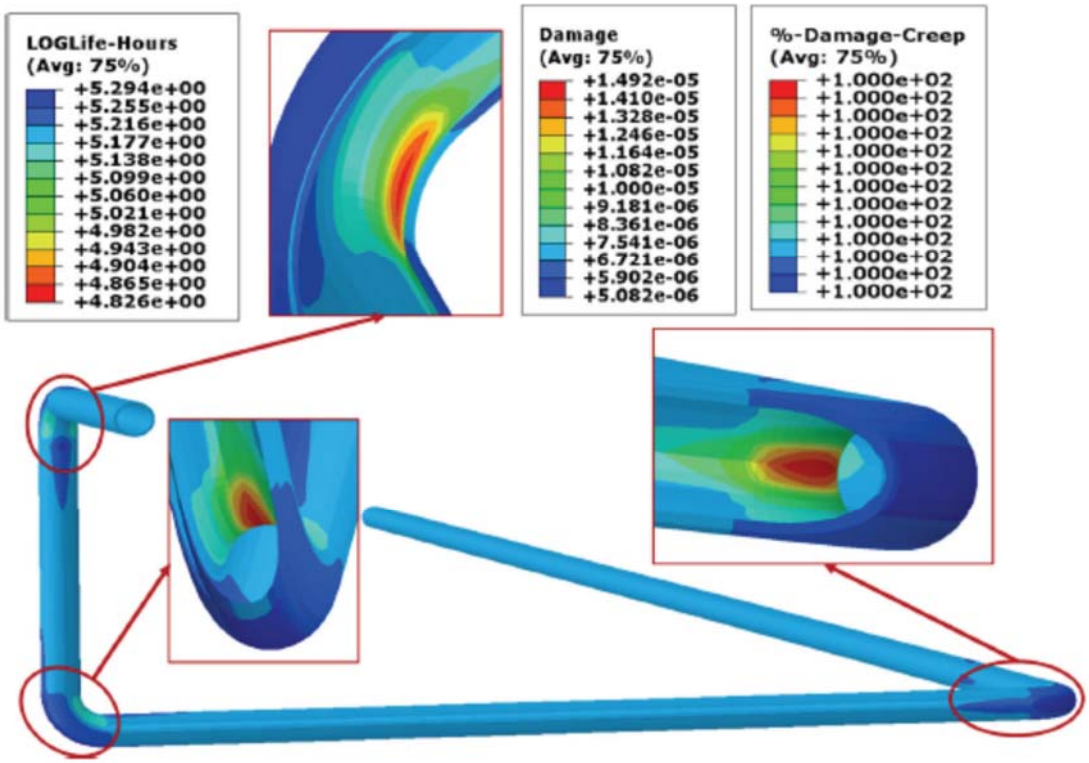

Fig. 16 Contour plot for creep life and damage for fine-machined finished surface

The useful life of the machined finished piping network under the specified operating condition is 7.10 years (61,802 h) and the maximum damage due to the dominant creep

failure is 1:617 X 10^{-5}, while the life for the fine-machined finished surface and the maximum damage are 7.70 years (66,989 h) and 1:492 X 10^{-5}, respectively. The creep–fatigue interaction curve, shown in Fig. 17 computed by fe-safe/TURBOlife, shows that the failure is strictly due to creep and this can be attributed to the lack of extensive plastic deformation during operation [36]. Also, the graph of percentage creep damage as a function of time is shown in Fig. 18. It was observed that the percentage creep damage increases with increase in operational time until the pipe failed completely after 7.10 years for the machined finished surface and 7.70 years for the fine-machined finished surface as shown in Table 4. Both failures were observed to occur at the elbow's intrados of the piping network. Further to the analytical validation of results performed below, it is interesting to note that these life failure years are realistic and consistent with actual data.

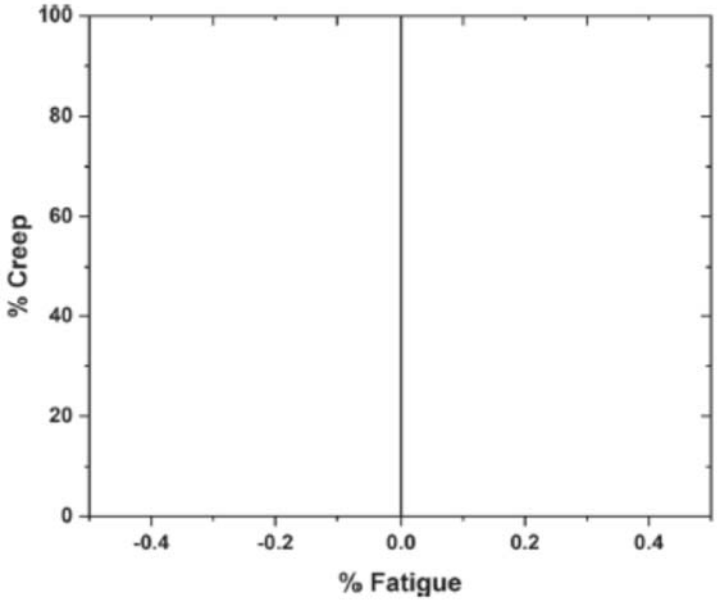

Fig. 17 Creep–fatigue interaction graph

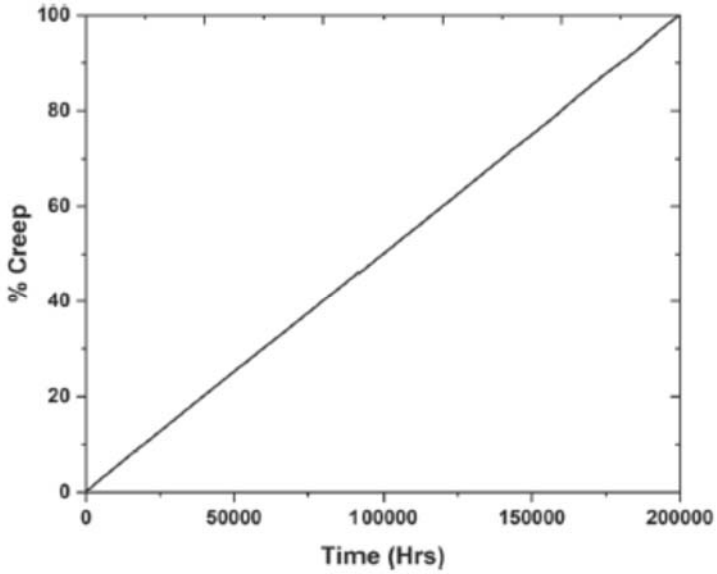

Fig. 18 % Creep damage as a function of time plot interaction graph

Table 4 Worst creep life and damage of P91 steam piping in operation under different surface finishing

Models	Machined finish			Fine-machined finish		
	Loglife	Life (Years)	Damage ($\times 10^{-5}$)	Loglife	Life (Years)	Damage ($\times 10^{-5}$)
Modified sine creep	4.791	7.10	1.617	4.826	7.70	1.492

Analytical Validation

The complex nature of the piping network and the lack of established equations for the determination of thermo-mechanical stress developed in a complex piping network has made it impossible to validate the creep rate of the piping network. However, the creep rate at the straight region of the piping network can be analytically validated due to the availability of established equations for the determination of thermo-mechanical stresses developed in thick-walled cylinders. In this work, the thermo-mechanical stress developed in the straight region of the piping network was determined using Eqs 1, 2, 3, 4, 5, 6, 7, 8 and 9, while the stress value obtained was used alongside the specified material constants in the creep model specified in Eq 3 to determine the creep strain rate under the stated operating condition. Good correlation was observed between the numerically computed and analytically calculated results. The simulated result for the creep strain rate for the straight region of the piping network is shown in Fig. 14, and the results for the comparison between the analytically calculated and numerically simulated creep rates for the straight region of the piping network are shown in Table 5.

Table 5 Comparison of analytical and simulated creep rates of a straight region of the piping network

Creep models	Analytical creep rate (h^{-1})	Simulated creep rate (h^{-1})	Deviation (%)
Modified sine creep	1.120×10^{-7}	1.114×10^{-7}	0.54

Conclusion

The possibility of failure of P91 steam piping network subjected to a typical power plant operational cycle due to creep–fatigue interaction fatigue interaction was investigated using FE software, Abaqus CAE/2019 in conjunction with fe-safe/TURBOlife. The creep stress and creep rate of the piping network were determined in Abaqus, while the creep damage and useful life were determined using fesafe/TURBOlife software. The outcome of the entire analysis shows that the failure of the piping network under the specified operating conditions is strictly due to creep, and there is no interaction between creep and fatigue due to the lack of the required extensive plastic strain to initiate fatigue failure. Also, the start-up and shutdown cycles had significant effect of the creep life of the piping network since the operating cycles prevented the piping network from experiencing the required stress relaxation which aids in prolonging creep life. The maximum creep stress and strain were obtained at the intrados of the piping network's elbow, thus indicating that the intrados is the region most prone to failure due to creep in the entire piping network. Lastly,

a strong correlation was obtained between the numerically simulated and the analytically calculated creep rates for the straight region of the piping network.

Acknowledgments

This research has been profusely supported by Tshwane University of Technology and the University of Pretoria, South Africa. Also, the authors greatly appreciate the unending support of Eskom Power Plant Engineering Institute (Republic of South Africa).

References

1. H. Jing et al., Finite element simulation of creep–fatigue crack growth behavior for P91 steel at 625°C considering creep–fatigue interaction. Int. J. Fatigue **98**, 41–52 (2017)
2. V. Shlyannikov, A. Tumanov, N.J.E.F.M. Boychenko, A creep stress intensity factor approach to creep–fatigue crack growth. Eng. Fract. Mech. **142**, 201–219 (2015)
3. X. Zhang et al., Creep–fatigue endurance of 304 stainless steels. Theor. Appl. Fract. Mech. **71**, 51–66 (2014)
4. R.J.F. Hales, A quantitative metallographic assessment of structural degradation of type 316 stainless steel during creep–fatigue. Fatigue Fract. Eng. Mater. Struct. **3**(4), 339–356 (1980)
5. K. Sadananda, P.J.M. Shahinian, Effect of environment on crack growth behavior in austenitic stainless steels under creep and fatigue conditions. Metall. Trans. A **11**(2), 267–276 (1980)
6. J.-F. Wen et al., Simulations of creep crack growth in 316 stainless steel using a novel creep-damage model. Eng. Fract. Mech. **98**, 169–184 (2013)
7. B. Fournier et al., Creep–fatigue–oxidation interactions in a 9Cr–1Mo martensitic steel. Part I: effect of tensile holding period on fatigue lifetime. Int. J. Fatigue **30**(4), 649–662 (2008)
8. Dassault Simulia Systemes, *fe-safe/TURBOlife User Manual* (Providence, RI, 2017), p. 122
9. L. Zhao et al., Analysis of creep crack growth behavior of P92 steel welded joint by experiment and numerical simulation. Mater. Sci. Eng. **558**, 119–128 (2012)
10. T. Hyde et al., Creep crack growth data and prediction for a P91 weld at 650°C. Int. J. Press. Vessels Pip. **87**(12), 721–729 (2010)
11. M. Saber, W. Sun, T.J.E.F.M. Hyde, Numerical study of the effects of crack location on creep crack growth in weldment. Eng. Fract. Mech. **154**, 72–82 (2016)
12. Z. Ding et al., Modeling of fatigue crack growth in a pressure vessel steel Q345R. Eng. Fract. Mech. **135**, 245–258 (2015)
13. V. Bolotin, I.J.P. Belousov, Early fatigue crack growth as the damage accumulation process. Probab. Eng. Mech. **16**(4), 279–287 (2001)
14. H. Li, H. Yuan, X. Li, Assessment of low cycle fatigue crack growth under mixed-mode loading conditions by using a cohesive zone model. Int. J. Fatigue **75**, 39–50 (2015)
15. R.M. Code, *Design and Construction Rules for Mechanical Components of FBR Nuclear Islands and High Temperature Applications, Appendix A16, Tome I*, vol. Z (AFCEN, Paris, 2007)

16. A. Boiler, *Rules for Construction of Pressure Vessels* (American Society of Mechanical Engineers, New York, 2013)
17. R.A. Ainsworth, *R5: Assessment Procedure for the High Temperature Response of Structures* (British Energy Generation Ltd, 2003)
18. M.J. Chrzanowski, Use of the damage concept in describing creep–fatigue interaction under prescribed stress. Int. J. Mech. Sci. **18**(2), 69–73 (1976)
19. L. Xu et al., A novel creep–fatigue interaction damage model with the stress effect to simulate the creep–fatigue crack growth behavior. Int. J. Mech. Sci. **130**, 143–153 (2017)
20. D. Annaratone, Cylinders under internal pressure. Press. Vessel Des. 47–125 (2007)
21. B. Kanlıkama, A. Abuşoğlu, İ.H. Güzelbey, Coupled thermoelastic analysis of thick-walled pressurized cylinders. Int. J. Energy Power Eng. **2**(2), 60–68 (2013)
22. A. Kandil, A. El-Kady, A. El-Kafrawy, Transient thermal stress analysis of thick-walled cylinders. Int. J. Mech. Sci. **37**(7), 721–732 (1995)
23. V. Pesonen, *Online Creep and Fatigue Monitoring in Power Plants* (2014)
24. F. Garofalo, An empirical relation defining the stress dependence of minimum creep rate in metals. Trans. Metall. Soc. AIME **227**(2), 351–355 (1963)
25. J.M. Montes, F.G. Cuevas, J. Cintas, New creep law. J. Mater. Sci. Technol. **3**(28), 377–379 (2012)
26. R. Skelton, D.J. Gandy, Creep–fatigue damage accumulation and interaction diagram based on metallographic interpretation of mechanisms. Mater. High Temp. **25**(1), 27–54 (2008)
27. J.-F. Wen, S.-T. Tu, A multiaxial creep-damage model for creep crack growth considering cavity growth and microcrack interaction. Eng. Fract. Mech. **123**, 197–210 (2014)
28. J. Lemaitre, A. Plumtree, Application of damage concepts to predict creep–fatigue failures. J. Eng. Mater. Technol. **101**(3), 284–292 (1979)
29. W. Ramberg, W.R. Osgood, Description of stress–strain curves by three parameters. Nasa Scientific and Technical Facility Report (1943), pp. 1–32
30. R. Lagneborg, R.J.M.T. Attermo, The effect of combined low-cycle fatigue and creep on the life of austenitic stainless steels. Metall. Trans. **2**(7), 1821–1827 (1971)
31. Dassault Simulia Systeme, *ABAQUS 6.13 User's Manual* (Providence, RI, 2013)
32. T. Rasiawan, *The Influence of Prior Creep Damage on the Fracture Localisation in X20 CrMoV12-1 Cross-Weld Creep Tests* (University of Cape Town, Cape Town, 2017)
33. Pyrogel-XTE-Datasheet, *High-Performance Aerogel Insulation for Industrial and Commercial Applications*
34. S. Salifu et al., Thermo-mechanical stress simulation of unconstrained region of straight X20 steam pipe. Proc. Manuf. **35**, 1330–1336 (2019)
35. Y. Gorash, D.J.O.E. MacKenzie, On cyclic yield strength in definition of limits for characterisation of fatigue and creep behaviour. Open Eng. **7**(1), 126–140 (2017)
36. M.E. Fine, Y.W. Chung, *Fatigue Failure in Metals*, vol. 19 (ASM International, 1996)